

Field-induced quantum spin-1/2 chains and disorder in $\text{Nd}_2\text{Zr}_2\text{O}_7$

J. Xu,^{1,2,*} A. T. M. N. Islam,¹ I. N. Glavatsky,¹ M. Reehuis,¹ Jens-Uwe Hoffmann,¹ and B. Lake^{1,2,†}

¹*Helmholtz-Zentrum Berlin für Materialien und Energie GmbH, Hahn-Meitner Platz 1, D-14109 Berlin, Germany*

²*Institut für Festkörperphysik, Technische Universität Berlin, Hardenbergstraße 36, D-10623 Berlin, Germany*

(Dated: August 6, 2018)

We present single crystal diffuse neutron scattering study on the quantum spin ice candidate $\text{Nd}_2\text{Zr}_2\text{O}_7$ pyrochlore in magnetic fields along the $(1\ 1\ 0)$ direction. Two-dimensional scattering sheets perpendicular to the $(1\ -1\ 0)$ direction were observed evidencing field-induced one-dimensional correlations and disorder. The pyrochlore lattice is completely separated into orthogonal sets of chains which is in strong contrast to classical spin ice and surprising for an “all-in-all-out” (AIAO) ordered magnet with a non-Ising Hamiltonian. Our mean field and Monte Carlo simulations reveal that the $(1\ 1\ 0)$ field induces a transition from the AIAO order to a “2-in-2-out” disordered state with interactions between the two sets of chains cancelled out, resulting in disorder and quantum spin-1/2 XYZ chains.

Introduction. Magnetic pyrochlore compounds display various fascinating physical phenomena due to geometrical frustration on the network of corner-sharing tetrahedra in the crystal structure [1]. The spin ice state with macroscopic degeneracy and monopole-like excitations is probably the most striking which was observed in $\text{Ho}_2\text{Ti}_2\text{O}_7$ and $\text{Dy}_2\text{Ti}_2\text{O}_7$ [2, 3]. It originates from a novel type of geometrical frustration where the local $[1\ 1\ 1]$ Ising anisotropy of the single ion forces the spins to point either into or out of the tetrahedra and frustrates the effective ferromagnetic (FM) interactions between the spins resulting in “2-in-2-out” spin configurations [4]. Classical spin ice can be melted by quantum fluctuations introduced by non-Ising terms in the spin Hamiltonian [5–7]. This leads to quantum spin ice which is a type of long-sought quantum spin liquid prominent for emergent massive many-body entanglement and fractionalized excitations with topological properties [8–10].

An external magnetic field introduces constraints that lift spin ice degeneracy partially or totally leading to new novel states. For the classical spin ice, it has been reported that a field along the $(1\ 1\ 1)$ crystallographic direction pins one fourth of the spins and confines the residual entropy within two-dimensional (2D) kagome layers resulting in a kagome ice state [11, 12]. A field along the $(1\ 1\ 0)$ direction reduces the three-dimensional (3D) system to a quasi-one-dimensional (quasi-1D) system yielding Ising ferromagnetic chains interacting through dipolar interactions [13–16].

The reasons for the appearance of these field-induced states are related to decompositions of the pyrochlore lattice with respect to the magnetic field directions and the symmetry of interactions. For example, for the $(1\ 1\ 0)$ field direction, the pyrochlore lattice can be viewed as being composed of one-dimensional chains parallel (α -chains) and perpendicular (β chains) to the $(1\ 1\ 0)$ direction [Fig. 1(a)]. The $(1\ 1\ 0)$ field polarizes the α chains but does not affect the β chains directly due to the local $[1\ 1\ 1]$ Ising anisotropy [Fig. 1(b)]. The effective interactions between the two sets of chains sum to

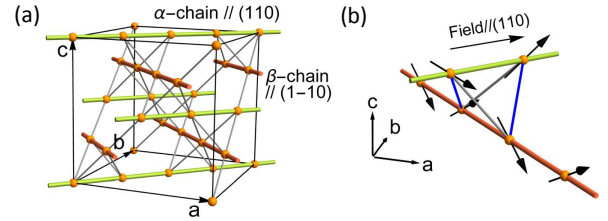


FIG. 1. (a) Pyrochlore lattices decomposed into chains parallel (α chains) and perpendicular (β chains) to the $(1\ 1\ 0)$ direction. (b) Polarized α chains in the $(1\ 1\ 0)$ field and non-collinear ferromagnetic order on the β chains (alternating “in/out” order with moments pointing along the local $[1\ 1\ 1]$ directions). The effective Ising FM interactions between the two types of chains are frustrated and cancelled out (the satisfied and unsatisfied bonds are shown in blue and grey, respectively).

zero as a result of the frustration of the interactions between α and β chains [Fig. 1(b)] [15–17]. The isolated β chains could show intra-chain non-collinear FM order with two possible directions for the net moment. However, the long-range dipolar interactions between the β chains were found to induce antiferromagnetic (AFM) inter-chain correlations or a $Q = X$ order (“X” corresponds points at e.g. $[0\ 0\ 1]$, $[0\ 0\ 3]$, $[0\ 1\ 1]$ in the reciprocal space) [4, 15–17].

The quantum counterparts of these field-induced novel states are expected to show in quantum spin ice which is more fascinating due to the inherent quantum dynamics instead of only thermal fluctuations in classical spin ice. It has been shown theoretically that quantum strings with monopoles at their ends appear in quantum spin ice in $(1\ 0\ 0)$ fields [18]. Recently, a 2D spin liquid state was predicted to show on the kagome layers in pyrochlores with dipolar-octupolar doublets in $(1\ 1\ 1)$ fields [19–21].

However, these field-induced quantum states in quantum spin ice have not been observed clearly in experiments due to the lack of proper quantum spin ice materials [22–26]. Recently, Nd-containing pyrochlores were

proposed in theory to be candidates for quantum spin ice and they are quite special because of the peculiar symmetry of the dipolar-octupolar crystal field ground state doublet of the Nd^{3+} ion [27]. The pseudospin-1/2 Hamiltonian has the form of the XYZ model which supports two distinct symmetry-enriched $U(1)$ quantum spin ice phases, i.e., dipolar and octupolar quantum spin ice states [27, 28]. Neutron scattering experiments on $\text{Nd}_2\text{Zr}_2\text{O}_7$ confirmed that the single-ion crystal field ground state is an Ising-anisotropic dipolar-octupolar doublet and the collective ground state was found to be an “all-in-all-out” (AIAO) order (Neel temperature $T_N=0.4$ K) [29, 30]. It shows dynamical spin ice correlations and quantum moment fragmentation where a parameterized spin Hamiltonian was proposed [31, 32]. The behaviors in fields have been studied with magnetization and susceptibility measurements and field-induced transitions were observed at critical fields ~ 0.1 T [29, 33]. Very recently, the ground state of $\text{Nd}_2\text{Zr}_2\text{O}_7$ in a (1 1 1) field was found to be a “3-in-1-out” state which shows remarkably dynamical kagome ice [34].

In this Communication, we study the ground state of $\text{Nd}_2\text{Zr}_2\text{O}_7$ in high (1 1 0) fields by means of single crystal diffuse neutron scattering. We find evidence for field-induced one-dimensional chains in $\text{Nd}_2\text{Zr}_2\text{O}_7$ even though the zero-field ground state is the AIAO AFM order rather than a spin ice state. These chains are supposed to be XYZ spin-1/2 chains with quantum dynamics, in contrast to the Ising spin chains realized in the classical spin ice. No features of inter-chain correlations are observed which is ascribed to the weak dipolar interactions between the β chains and the strong quantum fluctuations expected for this quantum chain.

Experimental. The single crystal was grown in a high temperature floating zone furnace (Crystal Systems Corp.) equipped with Xenon arc lamps and characterized by X-ray Laue diffraction, powder diffraction and magnetic measurements in the Quantum Materials Corelabs at Helmholtz-Zentrum Berlin (HZB) [35]. The AC susceptibility of this sample was reported in Ref. [33] which reveals an AFM ordering transition at 0.31 K, consistent with previous results on the powder and single crystal samples [29, 30]. A diffuse neutron scattering experiment was performed on the E2 diffractometer at HZB (neutron wavelength $\lambda = 2.38$ Å) with applied magnetic fields (0-2 T) along the (1 1 0) direction at 50 and 450 mK [36]. The (H -H L) reciprocal plane was measured with out-of-plane component along the (1 1 0) axis in the range [-0.1, 0.4]. A scattering pattern is also measured at 20 K in zero field which was subtracted as the background.

Results and analyses. Fig. 2 shows the three-dimensional diffuse neutron scattering data at 50 mK under a field of 0.5 T. We can see a strong two-dimensional scattering sheet perpendicular to the (1 -1 0) direction passing through the zero point. After integrating the data over the (1 1 0) axis, we clearly see streaks parallel

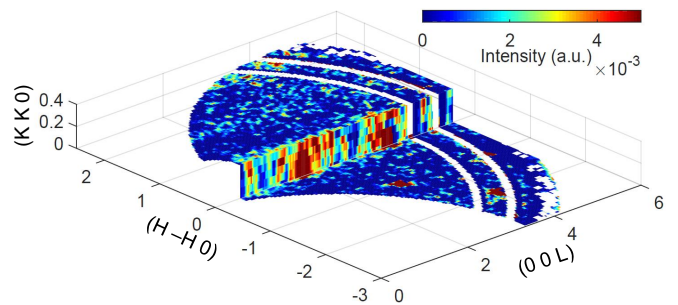


FIG. 2. Three-dimensional neutron diffuse scattering pattern in the reciprocal space at 50 mK in 0.5 T (1 1 0) field where the two-dimensional scattering planes perpendicular to (1 -1 0) direction are shown. The data collected at 20 K in zero field is subtracted as the background.

to the (0 0 L) axis passing through the points (0 0 0), (2 -2 0) and (-2 2 0) as shown in Figs. 3(a)-(c) [Fig. 3(a) shows the featureless zero field data]. These scattering sheets are related to the one-dimensional scattering of uncoupled β chains along the (1 -1 0) direction. The continuous scattering along the (0 0 1) and (1 1 0) directions signals a complete disorder between the β chains in $\text{Nd}_2\text{Zr}_2\text{O}_7$ in contrast to the classical spin ice materials for which broad $Q = X$ Bragg peaks were observed indicating significant inter-chain correlations [13, 14]. In addition, we also see strong Bragg peaks at [1 -1 1], [1 -1 3], [2 -2 4], (0 0 4) and especially at (0 0 2) where nuclear scattering is forbidden which are also observed for $\text{Dy}_2\text{Ti}_2\text{O}_7$ and $\text{Ho}_2\text{Ti}_2\text{O}_7$ in (1 1 0) fields and can be associated with the scattering of the polarized α chains [4, 13, 14].

Similar scattering patterns were observed for other fields and 450 mK as shown in Fig. 3 and the supplementary materials [35]. The intensity increased for higher fields but the peak width along the (1 -1 0) direction did not seem to change for the different fields as shown by the cuts through the data along the (H -H 0) axis [Fig. 3(d) and (h)]. The intra-chain correlation length ξ of the β chains was estimated by fitting the cuts along the (H -H 0) axis with a resolution-convoluted Lorentzian function of the Ornstein-Zernike form and it yields $\xi \sim 10$ Å suggesting a correlation length within one unit cell. This is very different from the classical spin ice which shows that the intra-chain correlation length increases up to 100 Å with increasing the field [13, 14]. This is attributed to the strong quantum fluctuations expected in $\text{Nd}_2\text{Zr}_2\text{O}_7$. This pattern persists above T_N at 450 mK but it is broader than at low temperature and thus indicates a shorter correlation length (~ 5 Å).

To gain more insights on the short-range correlations within the β chains, we calculated the structure factors of possible moment configurations. First, the magnetic moments should be along the local [1 1 1] directions respecting the single-ion Ising anisotropy. Second, with only the

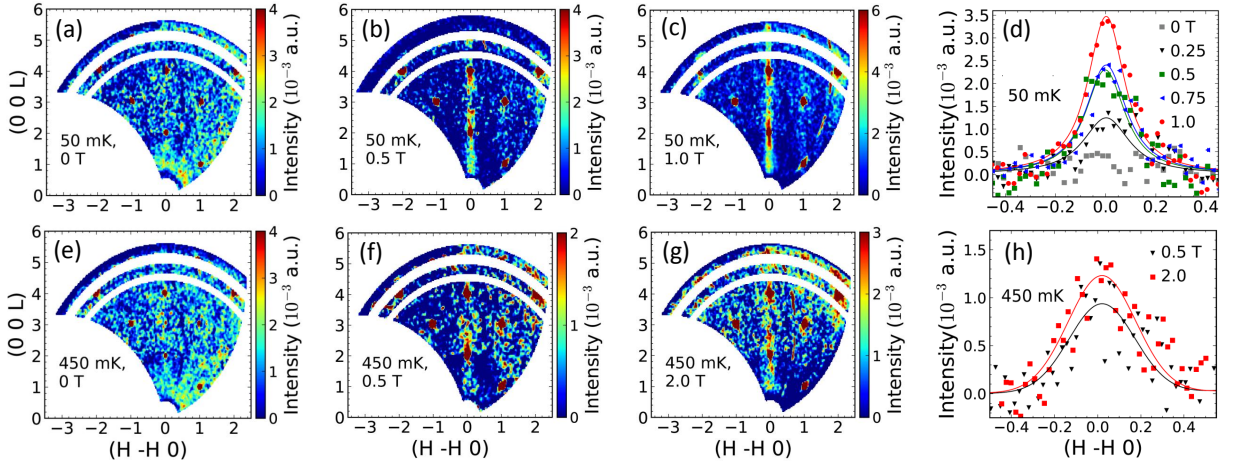


FIG. 3. (a)-(c) and (e)-(g): data collected at 50 and 450 mK in zero and several $(1\ 1\ 0)$ fields integrated along the $(K\ K\ 0)$ axis. (d) and (h): one-dimensional cut (points) along the $(H\ -H\ 0)$ axis with integration along the $(K\ K\ 0)$ and $(0\ 0\ L)$ axes (Bragg peaks are excluded) and fitting (lines) with a resolution-convoluted Lorentzian function. The data collected at 20 K in zero field is subtracted as the background for all the data.

nearest-neighbor interactions, a magnetic structure with zero propagation vector is most likely as indicated by the data. There are two types of magnetic structures possible: (i) a non-collinear FM order with alternating “in/out” magnetic moments along the chains as shown in Fig. 1(b); (ii) an AFM order with “all-in/all-out” moment configurations (flipping every second moment on the FM chain) [35]. Fig. 4(a) shows the calculated structure factor for a single FM β chain which is quite similar to the data. The AFM order produces a different pattern, thus excluding it as the possible solution (see the supplemental information) [35]. Therefore, the β chains show short-range FM intra-chain correlations.

As for the inter-chain disorder, it is counter-intuitive that a magnetic field could induce disorder in an ordered system even at such high fields. The observation for $\text{Nd}_2\text{Zr}_2\text{O}_7$ with the AIAO order as the zero-field ground state points out the unique properties of this compound. To study the origin, we performed mean-field calculations. The symmetry-allowed nearest-neighbor spin Hamiltonian with a magnetic field for the dipolar-octupolar doublet on the pyrochlore lattice is given as [27]

$$\mathcal{H} = \sum_{\langle i,j \rangle} J^x \tau_i^x \tau_j^x + J^y \tau_i^y \tau_j^y + J^z \tau_i^z \tau_j^z + J^{xz} (\tau_i^x \tau_j^z + \tau_i^z \tau_j^x) + hg_z \mu_B \sum_i \tau_i^z (\hat{z}_i \cdot \mathbf{n}) \quad (1)$$

where τ and J are the pseudospin and the exchange interactions respectively defined in local coordinate frames with the local $[1\ 1\ 1]$ crystallographic directions as the z axes, g_z is the only non-zero component of the Ising-anisotropic g tensor and h and \mathbf{n} are the magnitude and direction of the external field. Due to the peculiar sym-

metry of the dipolar-octupolar doublet, the interactions are uniform for every bond and the cross coupling J^{xz} can be removed by a global pseudospin rotation around the local y axes by an angle ϑ which leads to the XYZ model [27, 32]

$$\mathcal{H}_{XYZ} = \sum_{\langle i,j \rangle} [\tilde{J}^{\tilde{x}} \tilde{\tau}_i^{\tilde{x}} \tilde{\tau}_j^{\tilde{x}} + \tilde{J}^{\tilde{y}} \tilde{\tau}_i^{\tilde{y}} \tilde{\tau}_j^{\tilde{y}} + \tilde{J}^{\tilde{z}} \tilde{\tau}_i^{\tilde{z}} \tilde{\tau}_j^{\tilde{z}}] + hg_z \mu_B \sum_i (\tilde{\tau}_i^{\tilde{x}} \sin \vartheta + \tilde{\tau}_i^{\tilde{z}} \cos \vartheta) (\hat{z}_i \cdot \mathbf{n}), \quad (2)$$

where $\{\tilde{J}^{\tilde{x}}, \tilde{J}^{\tilde{y}}, \tilde{J}^{\tilde{z}}\}$ are the exchange parameters corresponding to the rotated pseudospin components $\{\tilde{\tau}^{\tilde{x}}, \tilde{\tau}^{\tilde{y}}, \tilde{\tau}^{\tilde{z}}\}$ defined in the rotated local frames and the magnetic moment is given by $m_i = g_z (\tilde{\tau}_i^{\tilde{x}} \sin \vartheta + \tilde{\tau}_i^{\tilde{z}} \cos \vartheta) \mu_B$ which lies along the local $[1\ 1\ 1]$ axes (details for this transformation are shown in Ref. [35]). Note that the non-Ising exchange interactions produce a mean field away from the Ising axis, which means that the pseudospins can rotate smoothly rather than flop when changing the magnetic field in contrast to classical spin ice. However, the magnetic moment is always exactly along the local $[1\ 1\ 1]$ directions due to the infinite Ising-anisotropy of the g tensor [29, 30].

In our mean-field calculations, the spins are treated as classical vectors [35] and the interaction parameters used are

$$\tilde{J}^{\tilde{x}} \approx 0.103, \tilde{J}^{\tilde{y}} \approx 0, \tilde{J}^{\tilde{z}} \approx -0.047 \text{ meV}, \quad (3)$$

$$g_z \approx 4.5, \vartheta \approx 0.83 \text{ rad},$$

which are suggested in Refs. [31, 32]. The ground state for this set of parameters is the AIAO order of the $\tilde{\tau}^{\tilde{z}}$ component though $|\tilde{J}^{\tilde{x}}|$ is much larger than $|\tilde{J}^{\tilde{z}}|$. This is because ice-like frustration happens for the FM $\tilde{J}^{\tilde{x}}$

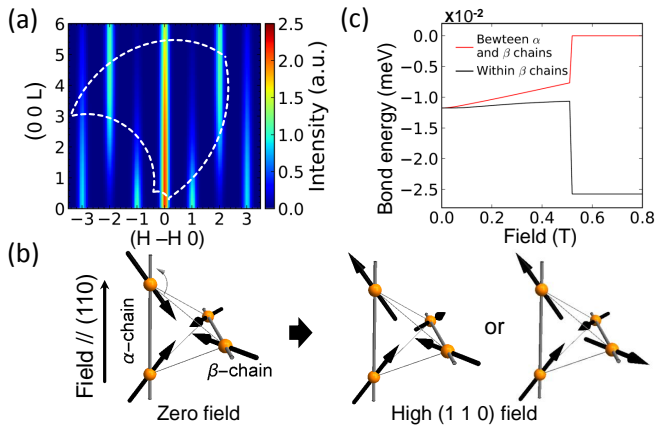


FIG. 4. (a) Calculated structure factor for a non-collinear “in/out” ferromagnetic chain along the (1 -1 0) direction as shown in Fig. 1(b) (including the magnetic form factor of Nd^{3+}). The dashed lines indicate the region measured in the experiment. (b) Schematic illustration of the field-induced transition showing the zero-field AIAO order and two equivalent induced orders with the net moments of the FM β chain reversed. (c) Average bond energies between α and β chains and within the β chains.

but not for the AFM \tilde{J}^z (here “FM” and “AFM” are based on the global crystal coordinate frame but they are the opposite regarding to pseudospins defined in the local frames). Starting from this state, the calculations show that the system undergoes a transition in increasing field which is consistent with the magnetic measurements though the calculated critical field ~ 0.5 T is higher than the experimental one (~ 0.1 T) [29, 35]. Fig. 4(b) illustrates the calculated moment configurations before and after the transition. In high fields, every second moment on the α chain is flipped in order to lower the Zeeman energy forming a field-polarized state. The β chains do not couple to the (1 1 0) field but they also show a FM order with an alternating “in/out” moment configuration which is exactly the magnetic correlations suggested by the neutron diffuse scattering data.

The above calculation explains not only the intra-chain FM order but also the inter-chain disorder for the β chains. Within the nearest-neighbor model, the α and β chains are interacting with each other but there is no direct interaction between chains of the same type. Each spin on the β chains is connected with four spins on two different α chains and two spins on the same β chains (vice versa for spins on the α chains) as shown in Fig. 1(a). After the field-induced transition, the spins on the α chains point alternately “in/out” of the tetrahedra (opposite to each other in terms of the local frames) and the spins on the β chains are subjected to an effective zero molecular field from the α chains because every spin on the β chains interacts with two pairs of “in/out” spins on α chains whose molecular fields cancel out.

This was confirmed by the mean field calculations.

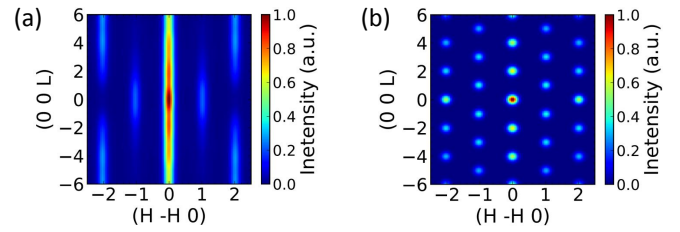


FIG. 5. Calculated scattering pattern for β (a) and α (b) chains based the states produced in the Monte Carlo simulations at 50 mK in the 1.0 T field along the (1 1 0) direction. The magnetic form factor of Nd^{3+} is included.

Fig. 4(c) shows that the average bond energies between α and β chains are exactly zero after the field-induced transition as for classical spin ice with Ising interactions. Therefore the β chains are effectively isolated. Finally the intra-chain exchange interactions of the β chains with the dominant ferromagnetic \tilde{J}^x term lead to FM intra-chain correlations with spins alternating along the positive and negative local \tilde{x} directions (an effective AFM order in terms of the pseudospin defined in the local frames). Due to the crystal symmetry, the net moment of a FM β chain could be parallel or antiparallel to the chain direction and the inter-chain disorder arises naturally in the absence of inter-chain interactions. On the other hand, the FM intra-chain correlations of the β chains evidenced by the data reveal that a FM term (either \tilde{J}^x or \tilde{J}^z) is dominant in the spin Hamiltonian of $\text{Nd}_2\text{Zr}_2\text{O}_7$ which supports the analyses of the inelastic neutron scattering data in Refs. [31, 32] and provides a constraint for the determination the exchange parameters. Although the FM term is frustrated in zero field, the frustration is relieved within the chains after the field-induced transition by the realization of the FM intra-chain correlations as shown by the lowering of the intra-chain bond energy in Fig. 4(c).

To verify this scenario suggested by the mean-field calculation and examine the effects of thermal fluctuations, we performed single-spin-flip Metropolis Monte Carlo (MC) simulations at finite temperatures using the SPINW MATLAB Package by implementing our own codes [37]. The simulations were carried out on a $10 \times 10 \times 10$ supercell of the pyrochlore unit cell (totally 16000 spins) with periodic boundary conditions. The details are given in the supplementary materials [35]. Fig. 5 shows the neutron scattering patterns of the α and β chains calculated separately based on the spin configurations produced in the MC simulations at 50 mK in the (1 1 0) field of 1 T. The scattering pattern of the β chains shows continuous scattering which agrees well with the data. The polarized α chains yield a scattering pattern consisting of Bragg peaks which is also consistent with the field-induced Bragg peaks observed and confirms that these peaks are due to the Bragg diffraction of the polarized α chains. Therefore, the MC simulation confirms

the field-induced 1D correlations and disorder.

Nevertheless, the current analyses are based on the nearest-neighbor model, and further-neighbor interactions would introduce inter-chains correlations as in the classical dipolar spin ice [4, 13–17]. The long-range dipolar interactions contribute ~ 0.01 K to the second nearest neighbor interactions in $\text{Nd}_2\text{Zr}_2\text{O}_7$ and are much weaker than the nearest-neighbor interactions and are much lower than the lowest temperature measured. Therefore the system is essentially one-dimensional in an applied magnetic field along (1 1 0).

Having established the existence of one-dimensional magnetism in $\text{Nd}_2\text{Zr}_2\text{O}_7$ in high (1 1 0) fields, we now consider the properties of the magnetic chains. Inherited from the parent system with the dipolar-octupolar spin Hamiltonian, the chains in $\text{Nd}_2\text{Zr}_2\text{O}_7$ are supposed to be XYZ spin-1/2 chains. The classical ground state is the ferromagnetic order of the $\tilde{\tau}^{\tilde{x}}$ component for the current Hamiltonian. However, it is well-known that due to the low-dimensionality, the classical ordered ground state is destroyed by thermal and quantum fluctuations. This is exactly what we found here, only short-range FM correlations within the β chains. One-dimensional spin-1/2 chains are famous for emergent fractionalized excitations [38, 39]. It will be very interesting to study the excitation spectrum within the β chains by using inelastic neutron scattering. It is remarkable that the excitations are not expected to be affected by the (1 1 0) field due to the Ising anisotropy and preserve their original properties in the (1 1 0) field. In addition, the possible further-neighbor inter-chain and intra-chain couplings and long-range dipolar interactions may introduce more interesting physics than the conventional one-dimensional quantum magnets.

Summary. We find field-induced one-dimensional quantum chains in the AIAO ordered pyrochlore $\text{Nd}_2\text{Zr}_2\text{O}_7$ in (1 1 0) fields by using single crystal neutron diffuse scattering. It is attributed to bond frustration and interaction cancellation which originate from the combined effect of single-ion anisotropy, dipolar-octupolar Hamiltonian and the lattice geometry. The first observation of 1D quantum magnetism on the pyrochlore lattice here provides a possibility to study one-dimensional magnetism on the pyrochlore lattice and could stimulate more theoretical and experimental studies on the field-induced behaviors in quantum spin ice and the emergent low-dimensional magnetism.

We thank O. Benton, Y.-P. Huang, M. Hermele, S. T. Bramwell, A. T. Boothroyd for helpful discussions. We acknowledge Helmholtz Gemeinschaft for funding via the Helmholtz Virtual Institute (Project No. VH-VI-521).

[†] bella.lake@helmholtz-berlin.de

- [1] J. S. Gardner, M. J. P. Gingras, and J. E. Greedan, *Rev. Mod. Phys.* **82**, 53 (2010).
- [2] T. Fennell, P. P. Deen, A. R. Wildes, K. Schmalzl, D. Prabhakaran, A. T. Boothroyd, R. J. Aldus, D. F. McMorrow, and S. T. Bramwell, *Science* **326**, 415 (2009).
- [3] D. J. P. Morris, D. A. Tennant, S. A. Grigera, B. Klemke, C. Castelnovo, R. Moessner, C. Czternasty, M. Meissner, K. C. Rule, J.-U. Hoffmann, K. Kiefer, S. Gerischer, D. Slobinsky, R. S. Perry, *Science* **326**, 411 (2009).
- [4] M. J. Harris, S. T. Bramwell, D. F. McMorrow, T. Zeiske, and K. W. Godfrey, *Phys. Rev. Lett.* **79**, 2554 (1997).
- [5] S. Onoda and Y. Tanaka, *Phys. Rev. Lett.* **105**, 047201 (2010).
- [6] S. Onoda and Y. Tanaka, *Phys. Rev. B* **83**, 094411 (2011).
- [7] J. G. Rau and M. J. P. Gingras, *Phys. Rev. B* **92**, 144417 (2015).
- [8] L. Savary and L. Balents, *Rep. Prog. Phys.* **80**, 016502 (2017).
- [9] M. J. P. Gingras and P. A. McClarty, *Rep. Prog. Phys.* **77**, 056501 (2014).
- [10] L. Balents, *Nature* **464**, 199 (2010).
- [11] K. Matsuhira, Z. Hiroi, T. Tayama, S. Takagi, and T. Sakakibara, *J. Phys.: Condens. Matter.* **14**, L559 (2002).
- [12] Y. Tabata, H. Kadowaki, K. Matsuhira, Z. Hiroi, N. Aso, E. Ressouche, and B. Fåk, *Phys. Rev. Lett.* **97**, 257205 (2006).
- [13] T. Fennell, O. A. Petrenko, B. Fåk, J. S. Gardner, S. T. Bramwell, and B. Ouladdiaf, *Phys. Rev. B* **72**, 224411 (2005).
- [14] J. P. Clancy, J. P. C. Ruff, S. R. Dunsiger, Y. Zhao, H. A. Dabkowska, J. S. Gardner, Y. Qiu, J. R. D. Copley, T. Jenkins, and B. D. Gaulin, *Phys. Rev. B* **79**, 014408 (2009).
- [15] J. P. C. Ruff, R. G. Melko, and M. J. P. Gingras, *Phys. Rev. Lett.* **95**, 097202 (2005).
- [16] S. Yoshida, K. Nemoto, and K. Wada, *J. Phys. Soc. Jpn.* **73**, 1619 (2004).
- [17] R. G. Melko and M. J. P. Gingras, *J. Phys.: Condens. Matter* **16**, R1277 (2004).
- [18] Y. Wan and O. Tchernyshyov, *Phys. Rev. Lett.* **108**, 247210 (2012).
- [19] J. Carrasquilla, Z. Hao, and R. G. Melko, *Nat. Commun.* **6**, 7421 (2015).
- [20] Y.-P. Huang and M. Hermele, *Phys. Rev. B* **95**, 075130 (2017).
- [21] T. A. Bojesen and S. Onoda, *Phys. Rev. Lett.* **119**, 227204 (2017).
- [22] K. A. Ross, L. Savary, B. D. Gaulin, and L. Balents, *Phys. Rev. X* **1**, 021002 (2011).
- [23] L. D. C. Jaubert, O. Benton, J. G. Rau, J. Oitmaa, R. R. P. Singh, N. Shannon, and M. J. P. Gingras, *Phys. Rev. Lett.* **115**, 267208 (2015).
- [24] L. Pan, S. K. Kim, A. Ghosh, C. M. Morris, K. A. Ross, E. Kermarrec, B. D. Gaulin, S. M. Koohpayeh, O. Tchernyshyov and N. P. Armitage, *Nat. Commun.* **5**, 4970 (2014).
- [25] K. Kimura, S. Nakatsuji, J. J. Wen, C. Broholm, M. B. Stone, E. Nishibori, and H. Sawa, *Nat. Commun.* **4**, 1934 (2013).
- [26] J. J. Wen, S. M. Koohpayeh, K. A. Ross, B. A. Trump, T. M. McQueen, K. Kimura, S. Nakatsuji, Y. Qiu, D. M. Pajerowski, J. R. D. Copley, and C. L. Broholm, *Phys.*

* jianhui.xu@helmholtz-berlin.de

- Rev. Lett. **118**, 107206 (2017).
- [27] Y.-P. Huang, G. Chen, and M. Hermele, Phys. Rev. Lett. **112**, 167203 (2014).
- [28] Y.-D. Li and G. Chen, Phys. Rev. B **95**, 041106(R) (2017).
- [29] E. Lhotel, S. Petit, S. Guitteny, O. Florea, M. Ciomaga Hatnean, C. Colin, E. Ressouche, M. R. Lees, and G. Balakrishnan, Phys. Rev. Lett. **115**, 197202 (2015).
- [30] J. Xu, V. K. Anand, A. K. Bera, M. Frontzek, D. L. Abernathy, N. Casati, K. Siemensmeyer, and B. Lake, Phys. Rev. B **92**, 224430 (2015).
- [31] S. Petit, E. Lhotel, B. Canals, M. Ciomaga Hatnean, J. Ollivier, H. Mutka, E. Ressouche, A. R. Wildes, M. R. Lees, and G. Balakrishnan, Nat. Phys. **12**, 746 (2016).
- [32] O. Benton, Phys. Rev. B **94**, 104430 (2016).
- [33] L. Opherden, J. Hornung, T. Herrmannsdörfer, J. Xu, A. T. M. N. Islam, B. Lake, and J. Wosnitzer, Phys. Rev. B **95**, 184418 (2017).
- [34] E. Lhotel, S. Petit, M. C. Hatnean, J. Ollivier, H. Mutka, E. Ressouche, M. Lees, and G. Balakrishnan, arXiv preprint, arXiv:1712.02418 (2017).
- [35] Supplementary Materials
- [36] J.-U. Hoffmann and M. Reehuis, Journal of large-scale research facilities, **4**, A129 (2018).
- [37] S. Toth and B. Lake, J. Phys.: Condens. Matter **27**, 166002 (2015).
- [38] B. Lake, D. A. Tennant, C. D. Frost, and S. E. Nagler, Nature. Mater. **4**, 329 (2005).
- [39] A. K. Bera, B. Lake, F. H. L. Essler, L. Vanderstraeten, C. Hubig, U. Schollwöck, A. T. M. N. Islam, A. Schneidewind, and D. L. Quintero-Castro, Phys. Rev. B **96**, 054423 (2017).

Supplementary Information for “Field-induced quantum spin-1/2 chains and disorder in $\text{Nd}_2\text{Zr}_2\text{O}_7$ ”

EXPERIMENTAL DETAILS

The $\text{Nd}_2\text{Zr}_2\text{O}_7$ single crystals were grown by using the optic floating zone furnace in the Crystal lab in Helmholtz-Zentrum Berlin, Germany and characterized using X-ray powder diffraction (XRD) (Bruker-D8, $\text{Cu-K}\alpha$) at room temperature. Rietveld refinements were performed using the software Fullprof Suite [S1].

The magnetic susceptibility and magnetization measurements (above 2 K) were performed on the magnetic properties measurement system (Quantum Design) at MagLab, Helmholtz-Zentrum Berlin.

The neutron diffuse scattering experiment with applied magnetic field along the (1 1 0) direction was performed on the E2 diffractometer at Helmholtz-Zentrum Berlin. The incident neutron wavelength was 2.38 Å (PG002). The magnet VM-4 provided a vertical field perpendicular to the scattering plane and a dilution refrigerator was used to cool the sample down to 50 mK. The measurements were performed in fields of 0, 0.25, 0.5, 0.75, 1.0, 1.25, 1.5, 1.75 and 2.0 T for 50 mK and in fields of 0.5, and 2.0 T for 450 mK.

CRYSTALLOGRAPHY AND MAGNETIC PROPERTIES

The refined XRD pattern and crystallographic parameters are shown in Fig. S1 and Table S1, respectively. The results are consistent with the previous reports for the powder and single crystal samples [S2–S4].

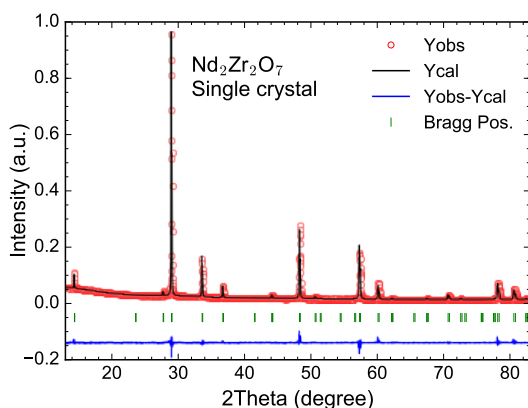


FIG. S1. X-ray powder diffraction pattern of single crystal $\text{Nd}_2\text{Zr}_2\text{O}_7$ at room temperature.

Fig. S2 shows the susceptibility of the single crystal sample of $\text{Nd}_2\text{Zr}_2\text{O}_7$ above 2 K. The susceptibility increases with decreasing temperature and shows no

TABLE S1. Crystallographic parameters of the single crystal of $\text{Nd}_2\text{Zr}_2\text{O}_7$ obtained from the refinement of the X-ray diffraction pattern recorded at room temperature. The lattice parameter a , atomic coordinate $x_{\text{O}1}$, overall thermal factor B_{iso} and refinement quality parameters are shown.

a (Å)	$x_{\text{O}1}$	B_{iso}	R_{WP}	R_{Bragg}	χ^2
10.651(1)	0.3347(1)	0.53(3)	4.74	4.66	2.55

anomaly above 2 K. The $\chi(T)$ data were fitted by the Curie-Weiss law with the Van Vleck term $\chi(T) = \chi_0 + C/(T - \theta_p)$ for the temperature range $10 \text{ K} \leq T \leq 30 \text{ K}$. This yields $\theta_p = 0.270(13) \text{ K}$, $\mu_{\text{eff}} = 2.47(1) \mu_{\text{B}}/\text{Nd}$ and $\chi_0 = 3.5(1) \times 10^{-3} \text{ emu/mol Nd}$, which is consistent with those reported for powder and single crystal samples [S2–S4]. The positive θ_p indicates an effective ferromagnetic interaction between the Nd^{3+} moments though the sample shows an “all-in-all-out” antiferromagnetic order. This is a consequence of the dipolar-octupolar nature of the effective spin of the Nd^{3+} ion in pyrochlores [S5].

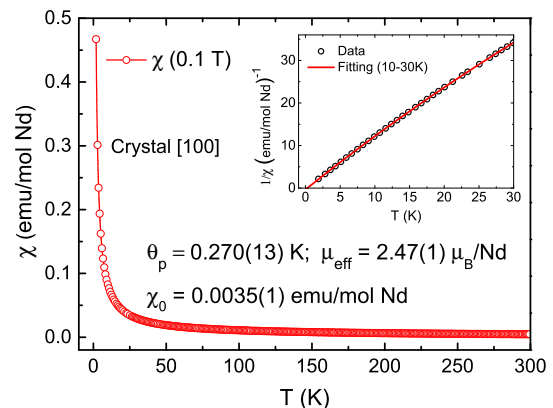


FIG. S2. Susceptibility of the single crystal $\text{Nd}_2\text{Zr}_2\text{O}_7$ with field 0.1 T applied along the [1 0 0] direction and the Curie-Weiss law fitting (inset).

AC susceptibility of this single crystal sample was shown in Ref. [S6]. The antiferromagnetic ordering temperature is $T_N \approx 310 \text{ mK}$. The transition temperature is lower than that of the powder sample (400 mK) shown in the specific heat data in Ref. [S7] and in the neutron diffraction data [S3, S4]. The crystal reported in Ref. [S3, S8] shows a transition temperature of 285 mK. This indicates that a small sample dependence is present for the $\text{Nd}_2\text{Zr}_2\text{O}_7$ single crystals. However the magnetic ground state of $\text{Nd}_2\text{Zr}_2\text{O}_7$ does not vary from sample to sample according to the neutron diffraction data of different samples [S3, S4, S8].

DIFFUSE NEUTRON SCATTERING WITH THE (1 1 0) FIELDS

Figure S3(a) shows the 3D neutron diffuse scattering data in 1 T at 50 mK where the (K K L) scattering sheet at $H = 0$ is presented. Fig. S3(b) and (c) shows (H -H L) layers of the data for vertical (K K 0) components with $K = 0$ and $K = 0.4$ r.l.u. measured in 1 T and 0.5 T fields at 50 mK, respectively. The $K = 0.4$ layers show no Bragg peaks but only streaks with similar intensity as in the layer at $K = 0$ and they show no clear variation of intensity along (0 0 L). Therefore, the scattering sheet clearly extends to at least $K = 0.4$ r.l.u. which suggests an upper limit 3 \AA for the inter-chain correlation length along (K K 0). It is smaller than the nearest-neighbor distance $\sqrt{2}/2a$ along (K K 0) between the β chains. Therefore, the scattering sheet is neither an effect of the vertical instrument resolution nor due to the very-short-range inter-chain correlations.

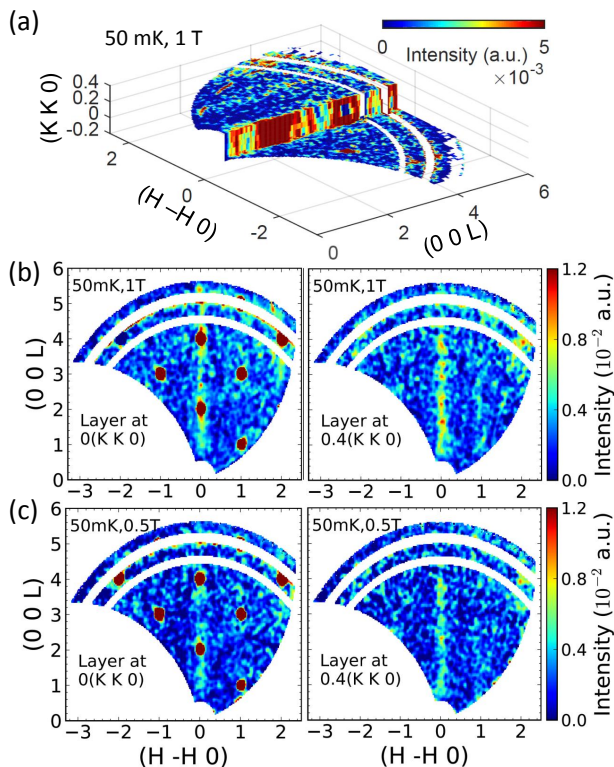


FIG. S3. (a) Three-dimensional neutron diffuse scattering data with a 1.0 T field along the (1 1 0) direction at 50 mK. (b) and (c): Data at 50 mK in 1.0 and 0.5 T fields showing the (H -H L) reciprocal plane with vertical (K K 0) components fixed at $K = 0$ and $K = 0.4$ r.l.u..

Figure S4 (a) and (b) shows the cuts of the data at 50 mK and 450 mK along the (H -H 0) axis with integration over the vertical (K K 0) component of $0.2 < K < 0.4$ (excluding the layers with Bragg peaks) which are compared with the calculated scattering pattern of a FM chain. In contrast to the featureless pattern

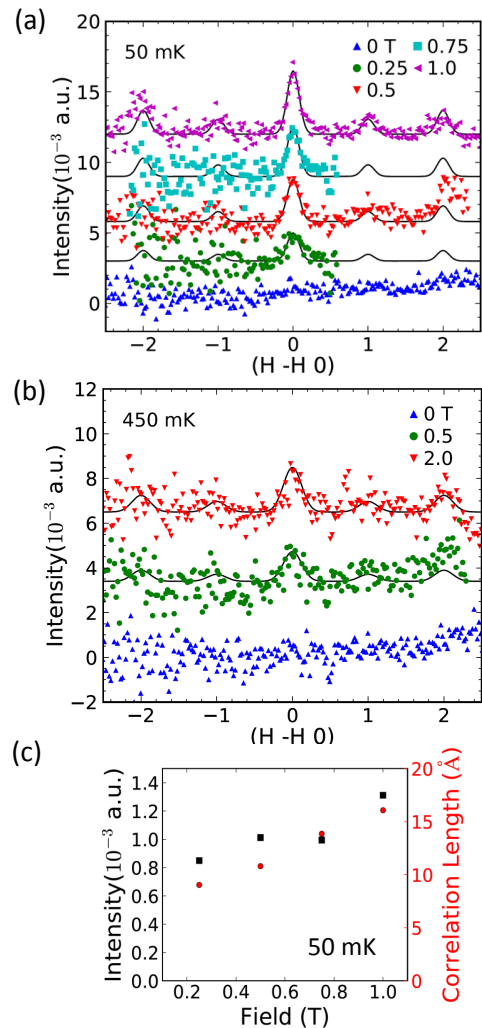


FIG. S4. (a) and (b): Cuts of the data at 50 mK and 450 mK along the (H -H 0) axis with integrating the (H -H L) layers with 0.2-0.4 (K K 0) vertical components (excluding the layers with Bragg peaks) and the black lines shows the scaled calculated scattering pattern for the FM chains convoluted with a Gaussian function. The data are shifted vertically by 0.003 unit successively for better visualization. (c) Intensity and correlation length at 50 mK in different fields estimated from fitting the peaks at $H = 0$ with a Lorentzian function convoluted with the resolution function. All the data are background-subtracted.

in zero field, the patterns in the (1 1 0) fields show peaks at $H = 0, \pm 1$ and ± 2 due to the scattering sheets, which is in agreement with the calculations. The intensity and the correlation length at 50 mK in different fields were estimated from fitting the peaks at $H = 0$ which were shown in Fig. S4(c). They show a weak increase as the field increases and do not change much in different fields.

Figures 3(a) and (e) in the main text show the zero field data at 50 and 450 mK which does not have a clearly structured pattern in contrast to the data measured in field. Note that there is a Bragg peak at (0 0 2) which is

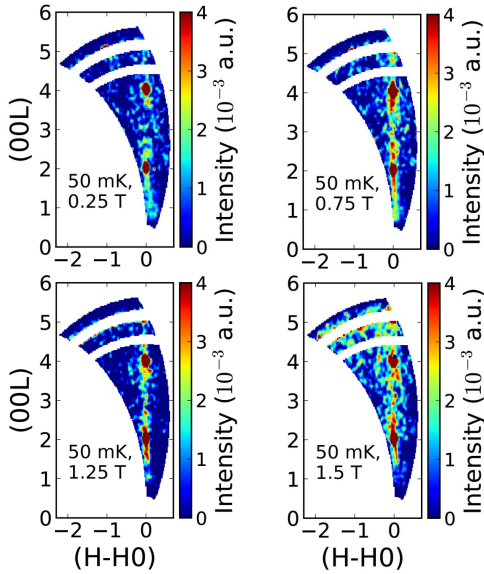


FIG. S5. Data at 50 mK in 0, 0.25, 0.75, 1.25 and 1.5 T fields and data at 450 mK in zero field integrated over the out-of-plane scattering with the wave vector component along (K K 0) in the range $[-0.1, 0.4]$. All the data are background-subtracted.

a forbidden position for nuclear scattering and it is possibly caused by multiple scattering which was also seen in $\text{Ho}_2\text{Ti}_2\text{O}_7$ [S9] (it exists also in the 20 K data). The nuclear peaks are stronger at the low temperatures than at 20 K due to the Debye-Waller factor and the magnetic Bragg scattering of the AIAO order [S3, S4].

Figure S5 shows data at 50 mK in 0.25, 0.75, 1.25 and 1.5 T fields. They all show a streak along the (0 0 L) direction. In fields higher than ~ 1 T, the diffuse scattering pattern gets blurred because there is a misalignment ~ 0.9 degree of the (H -H 0) axis and the field tends to polarize the β chains inducing long-range inter-chain ferromagnetic order. This was also shown by the intensity of the (0 0 2) peak as a function of the field in Fig. S6. The intensity of (0 0 2) increases with the field and shows a plateau at ~ 1 T indicating a nearly fully polarization of the α chains, consistent with the magnetization data [S3]. The intensity increases further in fields above 1 T indicating the polarizing of the β chains.

Figure S7 shows the one-dimensional cuts through the data along the (0 0 L) and (K K 0) axes. There is no clear modulation of the intensity of the diffuse scattering along the two axes which indicates uncorrelated chain scattering.

SCATTERING PATTERN OF AN ANTIFERROMAGNETIC CHAIN

Figure S8(a) shows the antiferromagnetic (AFM) β chain with the moments pointing "all-in/all-out" of the

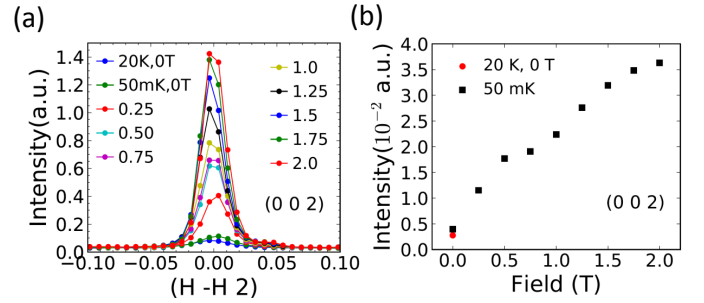


FIG. S6. (a) One-dimensional cuts through the data along the (H -H 2) axis integrated over a range of $[1.8, 2.2]$ for the (0 0 L) axis and a range of $[-0.1, 0.4]$ for the (K K 0) axis where the field dependence of the (0 0 2) Bragg peak is shown; (b) Field dependence of the integrated intensity of the (0 0 2) Bragg peak (without background subtraction).

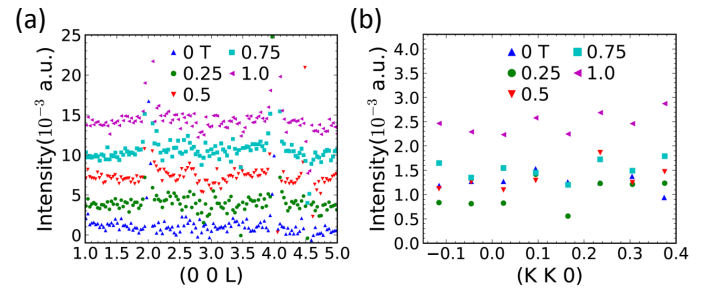


FIG. S7. One-dimensional cuts through the data at 50 mK in different fields: (a) cuts along the (0 0 L) axis integrated over a range of $[-0.2, 0.2]$ for the (H -H 0) axis and $[-0.1, 0.4]$ for the (K K 0) axis (shifted by 0.003 unit successively for a better visualization); (b) cuts along the (K K 0) axis integrated in the range $[-0.2, 0.2]$ for the (H -H 0) axis and $[0, 4]$ for the (0 0 L) axis but excluding the Bragg peaks (0 0 2) and (0 0 4). All the data are background-subtracted.

tetrahedra. There is a net moment perpendicular to the chain but no net moment along the chain direction. The scattering pattern of a single AFM β chain is shown in Fig. S8(b) which is quite different with the data.

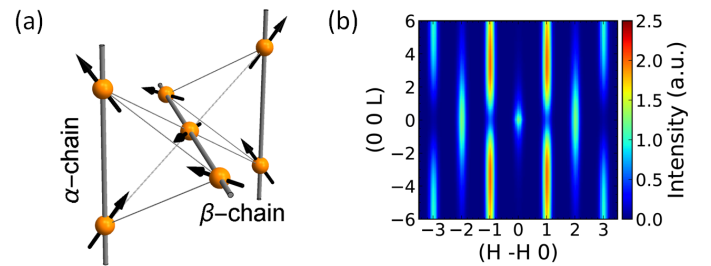


FIG. S8. (a) Polarized α chains and antiferromagnetic β chains; (b) Scattering pattern of an AFM β chain.

SPIN HAMILTONIAN AND MEAN FIELD CALCULATIONS

The general form of the pseudospin exchange Hamiltonian on the pyrochlore lattice is given by Eq. 1 in the local frames in the main text. The local frames for the four magnetic ions on a tetrahedron are defined with the local $[1\ 1\ 1]$ directions as the local z axes and the local y axes being chosen to keep the two-fold rotation invariance about the three axes that include the centre of the tetrahedron and are parallel to the global crystal a , b and c axes [S10, S11] (Fig. S9):

$$\begin{aligned} \hat{z}_0 &= \frac{1}{\sqrt{3}}(1, 1, 1) & \hat{x}_0 &= \frac{1}{\sqrt{6}}(-2, 1, 1) \\ \hat{z}_1 &= \frac{1}{\sqrt{3}}(1, -1, -1) & \hat{x}_1 &= \frac{1}{\sqrt{6}}(-2, -1, -1) \\ \hat{z}_2 &= \frac{1}{\sqrt{3}}(-1, 1, -1) & \hat{x}_2 &= \frac{1}{\sqrt{6}}(2, 1, -1) \\ \hat{z}_3 &= \frac{1}{\sqrt{3}}(-1, -1, 1) & \hat{x}_3 &= \frac{1}{\sqrt{6}}(2, -1, 1) \end{aligned}, \quad (\text{S1})$$

with $\hat{y}_i = \hat{z}_i \times \hat{x}_i$.

The pseudospin rotation (around the local y axis) is performed to remove the J^{xz} term which is a rotation around the local y axes [S5, S12] (Fig. S9)

$$\begin{aligned} \tilde{\tau}_i^{\tilde{x}} &= \tau_i^x \cos \vartheta + \tau_i^z \sin \vartheta, \\ \tilde{\tau}_i^{\tilde{y}} &= \tau_i^y, \\ \tilde{\tau}_i^{\tilde{z}} &= \tau_i^z \cos \vartheta - \tau_i^x \sin \vartheta, \\ \vartheta &= \frac{1}{2} \arctan\left(\frac{2J^{xz}}{J^{xx} - J^{zz}}\right). \end{aligned} \quad (\text{S2})$$

The relations between the exchange parameters in the initial local frames and in the rotated local frames are

$$\begin{aligned} J^x &= 0.5[(\tilde{J}^{\tilde{x}} + \tilde{J}^{\tilde{z}}) + (\tilde{J}^{\tilde{x}} - \tilde{J}^{\tilde{z}}) \cos(2\vartheta)], \\ J^y &= \tilde{J}^{\tilde{y}}, \\ J^z &= 0.5[(\tilde{J}^{\tilde{x}} + \tilde{J}^{\tilde{z}}) - (\tilde{J}^{\tilde{x}} - \tilde{J}^{\tilde{z}}) \cos(2\vartheta)], \\ J^{xz} &= 0.5(\tilde{J}^{\tilde{x}} - \tilde{J}^{\tilde{z}}) \sin(2\vartheta). \end{aligned} \quad (\text{S3})$$

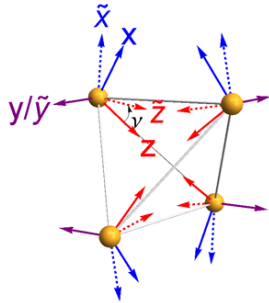


FIG. S9. Original $\{x, y, z\}$ (solid) and rotated $\{\tilde{x}, \tilde{y}, \tilde{z}\}$ (dashed) local frames.

In the mean field calculation, the spins are taken as classical vectors $\tau(\sin \theta_i \cos \phi_i, \sin \theta_i \sin \phi_i, \cos \theta_i)$ with $\tau = 1/2$ and θ_i and ϕ_i being the angles defining the direction of spins in the spherical coordinate frames based

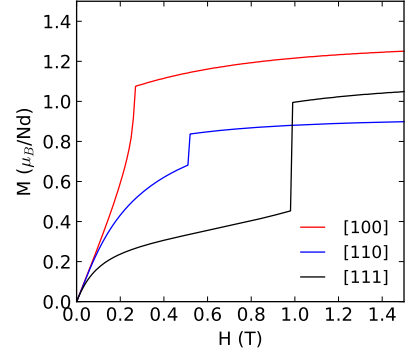


FIG. S10. Calculated magnetization for the three main cubic directions using the exchange parameters in Ref. [S5].

on the rotated local coordinate system. Two sets of exchange parameters for $\text{Nd}_2\text{Zr}_2\text{O}_7$ have been proposed which are quite similar with $\tilde{J}^{\tilde{x}}$ and $\tilde{J}^{\tilde{y}}$ being the largest and smallest terms [S5, S8, S13]. They do not give significantly different calculation results and here the parameters given in Ref. [S5] are used.

The mean-field calculations are performed by locally optimizing the energy by sweeping the field along the $(1\ 1\ 0)$ direction upwards and taking the spin configuration in the previous field as the start. Fig. S10 shows the calculated magnetization at zero temperature which exhibits field-induced transitions consistent with the measurements in Refs. [S3, S6]. The transition field H_c and the saturation values of magnetisation M_s is different from the measurements. They depends largely on the g -factor and the exchange parameters. The refined parameters reported in Ref. [S13] still fail to give an accurate modelling which calls for more efforts to determine the spin Hamiltonian of $\text{Nd}_2\text{Zr}_2\text{O}_7$.

After the field-induced transition for the $(1\ 1\ 0)$ direction, the spins on the β chains point along the positive and negative \tilde{x} directions (see Fig. S11). The magnetic moments are

$$\begin{aligned} m_i &= g_z(\tilde{\tau}_i^{\tilde{x}} \sin \vartheta + \tilde{\tau}_i^{\tilde{z}} \cos \vartheta) \mu_B \\ &= g_z \tilde{\tau}_i^{\tilde{x}} \sin \vartheta \mu_B \\ &= \pm 1/2 g_z \sin \vartheta \mu_B, \end{aligned} \quad (\text{S4})$$

which are along the local $[1\ 1\ 1]$ axes.

MONTE CARLO SIMULATIONS

The classical single-spin-flip Metropolis Monte Carlo simulations are performed based on the SPINW Matlab Package by implementing our own codes [S14]. The simulations of different supercell sizes confirmed that finite size effect was small. Finally, we used a $10 \times 10 \times 10$ supercell with periodic boundary conditions. At each temperature and/or field, $1 \times 10^5 \sim 5 \times 10^5$ Monte Carlo

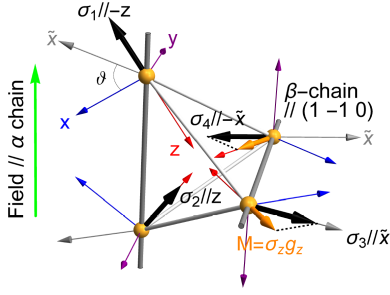


FIG. S11. Spin (black arrows) and moment (golden arrows) configurations in high (1 1 0) fields: the α chains are polarized with the spins and moments pointing into and out of the tetrahedra alternately (along the local z axes); the spins on the β chains points along positive and negative local \tilde{x} axes alternately producing moments directing out of and into the tetrahedra (the magnetic moment and spin are plotted with the same sign for simplicity). The original local frames and the rotated \tilde{x} local axes are also shown.

steps per spin were used for thermal equilibrium and $1 \times 10^5 \sim 5 \times 10^5$ Monte Carlo steps per spin for data collection while discarding $\sim 5 \times 10^3$ MC steps between successive data collection to reduce the correlation between measurements. To ensure that the results are fully thermally equilibrated, the simulations are started from different initial states, i.e., disordered, AIAO ordered and field polarized states. Two MC annealing procedures are considered: annealing in fields from high temperature to 0.05 K; sweeping the field at 0.05 K. To avoid freezing of the dynamics at low temperatures, the spins are moved in a cone around its present direction with the cone angle as a free parameter chosen to keep the acceptance rate $30 \sim 60\%$ for the most generic situations.

* jianhui.xu@helmholtz-berlin.de

† bella.lake@helmholtz-berlin.de

- [S1] J. Rodríguez-Carvajal, *Physica B: Condensed Matter* **192**, 55 (1993).
- [S2] M. C. Hatnean, M. R. Lees, O. A. Petrenko, D. S. Keeble, G. Balakrishnan, M. J. Gutmann, V. V. Klekovkina, and B. Z. Malkin, *Phys. Rev. B* **91**, 174416 (2015).
- [S3] E. Lhotel, S. Petit, S. Guitteny, O. Florea, M. Ciomaga Hatnean, C. Colin, E. Ressouche, M. R. Lees, and G. Balakrishnan, *Phys. Rev. Lett.* **115**, 197202 (2015).
- [S4] J. Xu, V. K. Anand, A. K. Bera, M. Frontzek, D. L. Abernathy, N. Casati, K. Siemensmeyer, and B. Lake, *Phys. Rev. B* **92**, 224430 (2015).
- [S5] O. Benton, *Phys. Rev. B* **94**, 104430 (2016).
- [S6] L. Opherden, J. Hornung, T. Herrmannsdörfer, J. Xu, A. T. M. N. Islam, B. Lake, and J. Wosnitzer, *Phys. Rev. B* **95**, 184418 (2017).
- [S7] S. Lutique, P. P. Javorský, R. J. M. Konings, A. C. G. van Genderen, J. C. van Miltenburg, and F. Wastin, *J. Chem. Thermodyn.* **35**, 955 (2003).

- [S8] S. Petit, E. Lhotel, B. Canals, M. Ciomaga Hatnean, J. Ollivier, H. Mutka, E. Ressouche, A. R. Wildes, M. R. Lees, and G. Balakrishnan, *Nat. Phys.* **12**, 746 (2016).
- [S9] J. P. Clancy, J. P. C. Ruff, S. R. Dunsiger, Y. Zhao, H. A. Dabkowska, J. S. Gardner, Y. Qiu, J. R. D. Copley, T. Jenkins, and B. D. Gaulin, *Phys. Rev. B* **79**, 014408 (2009).
- [S10] H. Yan, O. Benton, L. Jaubert, and N. Shannon, *Phys. Rev. B* **95**, 094422 (2017).
- [S11] S. Onoda and Y. Tanaka, *Phys. Rev. B* **83**, 094411 (2011).
- [S12] Y.-P. Huang, G. Chen, and M. Hermele, *Phys. Rev. Lett.* **112**, 167203 (2014).
- [S13] E. Lhotel, S. Petit, M. C. Hatnean, J. Ollivier, H. Mutka, E. Ressouche, M. Lees, and G. Balakrishnan, arXiv preprint, arXiv:1712.02418 (2017).
- [S14] S. Toth and B. Lake, *J. Phys.: Condens. Matter* **27**, 166002 (2015).